Proceedings of the Canadian Society for Mechanical Engineering International Congress
32nd Annual Conference of the Computational Fluid Dynamics Society of Canada
Canadian Society of Rheology Symposium
CSME-CFDSC-CSR 2025
May 25–28, 2025, Montréal, Québec, Canada

SPACING RATIO EFFECTS ON THE INTERFERENCE OF THREE-DIMENSIONAL TWIN SYNTHETIC JETS

Dorina Opoku-Mensah[1*], Akili Cyrus[1], Jerin John[1], Ebenezer E. Essel[1]
[1]Department of Mechanical, Industrial and Aerospace Engineering, Concordia University, Montreal, Canada
[*]d_opokum@live.concordia.ca

Abstract—A numerical study is performed to investigate the effects of spacing ratio ($s/d = 1.2, 2.0, 3.0$ and 4.0, where s is the center-to-center distance between the jets and d is the jet-exit diameter) on the mixing and turbulence characteristics of a circular twin synthetic jet (TSJ) using Improved Delay Detached Eddy Simulations (IDDES). The Reynolds number based on the maximum centerline jet-exit velocity was fixed at Re = 310 with an actuation frequency of 300 Hz. Both the phase-averaged and time-averaged results showed that the inner shear layers of the TSJ converge at the merging point, promoting interactions within the jets, which causes the jets to combine into a single jet further downstream. The merging and combined points increased linearly with the spacing ratio. However, the velocity decay rate of each jet generally decreased as the spacing ratio increased. For $s/d = 1.2$ and 2.0, the merging of the jets induced an axis-switching phenomenon, which was not observed for the larger spacing ratios. Q-criterion was used to examine the three-dimensional vortical structures associated with axis-switching and interference between the TSJ.

Keywords- synthetic jet, vortex ring, vortex merging

I. INTRODUCTION

A synthetic jet is a periodic flow created by an oscillating diaphragm or piston, generating a series of vortices [1]. The use of synthetic jet actuators (SJA) for flow control has become widespread over the past decade due to several technological advantages such as high jet momentum, ease of manufacturability and integration in fluid-thermal applications. For example, SJA has the potential to suppress flow separation and stall on wings of aircraft and blades of turbines, enhance industrial mixing, pollutant dispersion, cooling in heat transfer systems, and thrust vectoring in propulsion systems [1].

A traditional synthetic jet actuator consists of a cavity, a vibrating diaphragm, and an orifice through which the jet is expelled to the flow domain. Unlike conventional steady and pulsed jets, synthetic jets are formed from the working fluid within the domain and require no external fluid supply [2]. The periodic oscillation of the diaphragm causes the expulsion of fluid from the cavity in the expulsion phase and the ingestion of fluid into the cavity during the suction phase. This process results in the generation of a stream of vortices at the edges of the orifice which transfer momentum into the surrounding fluid. The interaction between these vortical structures with the external flow field can cause instabilities, altering the dynamics of the external flow [3].

A modification of a single synthetic jet is the twin synthetic jet (TSJ) which is generated by two parallel SJAs, as shown in Fig. 1. The mixing characteristics of the TSJ depend on important parameters such as the spacing ratio (s/d), stroke length (L_0) and Reynolds number (Re_0), where s is the center-to-center distance between the orifices and d is the orifice diameter. The stroke length (L_0) is the distance the expelled vortex ring travels during the expulsion phase, which is defined as:

$$L_o = U_o T \tag{1}$$

The Reynolds number of the synthetic jet is defined as:

$$Re_o = \frac{U_o d}{\nu} \tag{2}$$

where U_0 is the spatially averaged jet-exit velocity during the expulsion phase, T is the period of the actuation cycle of the SJA and ν is the fluid kinematic viscosity.

Fig. 1 shows the salient features of the time-averaged velocity field of a TSJ based on previous studies on twin steady jets [4]. The flow field can be divided into three distinct regions: converging region, merging region and combining region. The converging region is characterized by the converging and merging of the inner shear layers of twin jets. The merging region is characterized by the mixing and merging of the twin jets to form a single jet in the combined region. The converging region spans from the exit of the orifice to the merging point

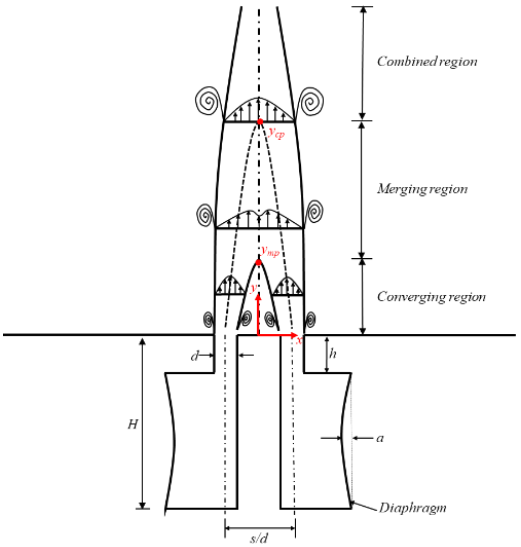

Figure 1. Schematic of dual synthetic jets in a quiescent flow and nomenclature used in the present study.

(y_{mp}), while the merging region spans from y_{mp} to the combined point (y_{cp}).

Unlike twin steady jets, the mixing and turbulence characteristics of TSJ issuing into a quiescent flow have received less attention. Most previous studies have focused on planar (2D) TSJ [5]. Smith and Glezer [5] performed an experimental study using particle image velocimetry (PIV) to investigate vortex merging and jet enhancement for 2D synthetic jets. They found that the combined jet formed from an in-phase 2D TSJ exhibits enhanced entrainment compared to a single 2D synthetic jet with a similar centerline velocity. Kim et al. [1] performed an PIV study to investigate the effects of spacing ratio (s/d = 1.2, 2.0, and 3.0) and stroke length (L_0/d = 13.7, 18.6, and 27.5) on the mixing characteristics of TSJ with round orifices. They found that merging and combined points decrease with decreasing spacing ratio and stroke length.

The objective of this study is to investigate the effects of spacing ratio on the unsteady flow interference of 3D TSJ. Four spacing ratios, $s/d = 1.2, 2.0, 3.0$ and 4.0 were studied using an Improved Delay Detached Eddy Simulation (IDDES).

II. NUMERICAL SETUP

A. Governing Equations and Turbulence Modelling

The synthetic jet in quiescent flow is governed by the three-dimensional unsteady incompressible Navier–Stokes equations written in tensor form as:

$$\frac{\partial u_i}{\partial x_i} = 0 \tag{3}$$

$$\left(\frac{\partial u_i}{\partial t} + \frac{\partial u_i u_j}{\partial x_j}\right) = -\frac{1}{\rho}\frac{\partial p}{\partial x_i} + \nu\frac{\partial^2 u_i}{\partial x_j \partial x_j} \tag{4}$$

where the indices, $i = 1, 2$ and 3, represent the x, y and z directions, respectively, t is the time, p is the pressure and the components of the instantaneous velocity vector are denoted by u_x, u_y and u_z, respectively.

All simulations in this study were performed using StarCCM+ with a hybrid second-order upwind scheme for convection terms and a second-order implicit scheme for time discretization. The turbulent flow is simulated using IDDES. IDDES uses RANS to model turbulence behaviour near the walls and LES for the unsteady turbulent flow characteristics away from the walls. The use of a hybrid approach, IDDES, reduces computational cost compared with complete LES. In this study, $k-\omega$ (SST) was used as the RANS model. To resolve the near-wall region, the dimensionless distance of the first cell from the walls $y^+ = \frac{u_\tau y_p}{\nu}$ was less than one, where y_p is distance normal to the wall and u_τ is the friction velocity. A timestep of $\Delta t = 1 \times 10^{-5} s$ was used for all the simulations to ensure a maximum Courant–Friedrichs–Lewy (CFL) number less than one.

B. Model Setup, Boundary, and Test Conditions

Fig. 2 shows the computational domain, and the grid refinement used for the simulations. Each of the SJA models has a cavity with a diameter of 30.8 mm and height of 4 mm, attached to a neck of length $h = 4$ mm and exit orifice diameter of $d = 1$ mm. The quiescent flow domain is 75 mm wide, 100 mm high and 100 mm long. The mesh for the entire flow domain consists of structured hexahedral elements with four refinement regions: a finer grid for the SJAs and jet-to-jet interference regions, an intermediate grid bounding the finer grid region, and a coarser mesh for the rest of the quiescent flow domain to reduce computational resources required for the unsteady 3D simulations.

A pressure outlet was assigned to the top surface of the flow domain, while the bottom surface was assigned a no-slip wall condition. The remaining four surfaces in the domain were treated as symmetry planes and no-slip wall conditions were assigned to the walls of the SJA domains. The SJA's diaphragm, in addition to its no-slip condition, was assigned an oscillatory motion based on a user-defined function (UDF) to simulate a vibrating diaphragm. The UDF calculates the instantaneous diaphragm displacement (s) as:

$$s = a\left(\frac{r}{r_o}\right)^2 (2\pi f t) \tag{5}$$

where a is the amplitude, r_o is the cavity radius, and r is the radial position of each grid. Each SJA was driven at $f = 300\,Hz$ with $a = 32\,\mu m$. The Reynolds number, based on the maximum centerline jet-exit velocity (U_{cl}) and d, was fixed at *Re* = 310.

As shown in Fig. 2, the Cartesian coordinate system adopted has the origin at the mid-span between the centers of the jet exits, with the *x*-axis corresponding to the spanwise direction, *y*-axis is in the streamwise direction and *z*-axis is in the crosswise direction.

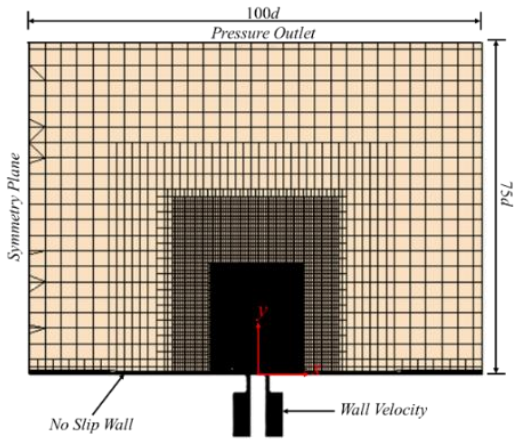

Figure 2. Computational domain and boundary condition.

The time-averaged and phase-averaged results reported herein were sampled after two flow-through cycles and over eight actuation cycles. During the data sampling, the residuals of continuity, momentum, turbulent kinetic energy, and dissipation rate equations were below 10^{-6}.

C. Grid Independence Study and Validation

Grid independence test was conducted using three levels of mesh resolution: coarse (1.0×10^6 cells), medium (2.0×10^6 cells), and fine (3×10^6 cells). The average centerline jet exit velocity was $U_{cl} = 4.65 \pm 0.1\ m/s$ for each mesh. The uncertainty in the mesh reduced from 0.2% to 0.1% as the mesh refinement increases from medium to fine grid. The medium grid was used for the present study as it provided higher spatial resolution than the coarse grid while requiring fewer computational resources than the fine grid.

Preliminary simulation using a single SJA, similar to Ho et al. [6], was performed and validated against existing experimental data from Feero *et al.* [10], prior to conducting the twin SJA simulations.

III. Results and Discussion

A. Phase-Averaged Flow Field

Contours of the phase-averaged normalized streamwise velocity (U_y/U_{cl}) at the symmetry plane ($z = 0$) for the two extreme cases ($s/d = 1.2$ and $s/d = 4$) are shown in Fig. 3. The maximum centerline jet-exit velocity, U_{cl} and d are used as the velocity and length scales, respectively. For brevity, the contours are shown for the peak expulsion (90°) and ingestion (270°) phases. The phases depict the streamwise evolution of the expelled jet from each SJA. For $s/d = 1.2$, the two jets merge near the exit and combine to form a single jet by the ingestion phase of the subsequent cycle. Beyond $y/d \geq 4$, the combined TSJ for $s/d = 1.2$ is evident as a thin strip of velocity region which decays and dismisses farther downstream. As spacing ratio increases, the interference between the TSJ is delayed as shown for the phases of $s/d = 4.0$. The contours show that the jets for $s/d = 4.0$ evolve independently while converging towards each other.

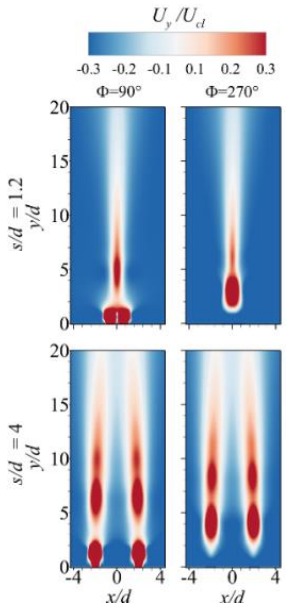

Figure 3. Contours of phase-averaged streamwise velocity of the twin synthetic jets for $s/d = 1.2$ and $s/d = 4.0$.

To examine the interactions within the shear layers of the TSJ, phase-averaged spanwise vorticity ($\omega_z d/U_{cl}$) contours are presented in Fig. 4. The positive and negative vorticity clusters represent counter-rotating vortex pairs (CVP) associated with vortex rings expelled at the exit of each SJA.

In $s/d = 1.2$, the contours demonstrate that the inner shear layers of the TSJ merge immediately near the exit plane, contrasting with the evolution of the shear layers in $s/d = 4.0$. Further downstream ($y/d \geq 2$), the two pairs of vorticity clusters near the exit transition into a single pair in $s/d = 1.2$, while in $s/d = 4$, the vorticity clusters remain distinct and gradually decay downstream. In agreement with the streamwise velocity contours, the vorticity in $s/d = 1.2$ stretches into two thin strips downstream of $y/d = 5$.

The 3D vortical structures of the TSJ are investigated using iso-surfaces of the phase-averaged Q-criterion, as shown in Fig. 5. These iso-surfaces are colored by the phase-averaged spanwise vorticity to depict the rotational direction of the vortical structures throughout each phase. For clarity, the stages of the TSJ evolution observed across the two phases are labelled I – VII. In each test case, the peak expulsion phase shows the formation of vortex rings near the TSJ exits (i.e., stage I). In $s/d = 1.2$, the expelled rings are attached to each other near the exit, whereas in $s/d = 4.0$, the rings are separated, as expected based on the increased spacing ratio. The subsequent development of the expelled ring (stage II) can be observed from the peak ingestion phase plots. In $s/d = 1.2$, the TSJ rings merge, and an interesting axis-switching phenomenon is observed, characterized by a reorientation of the combined ring's axis relative to the exit nozzles alignment. A similar axis-switching behavior was observed in $s/d = 2.0$ (not shown). This reorientation explains the transition of the

intense regions of streamwise velocity and spanwise vorticity in Figs. 3

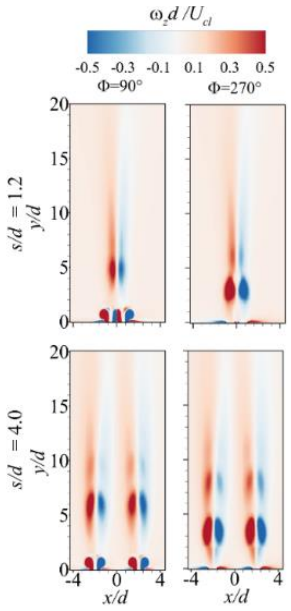

Figure 4. Contours of phase-averaged spanwise vorticity of the twin synthetic jets for $s/d = 1.2$ and $s/d = 4.0$.

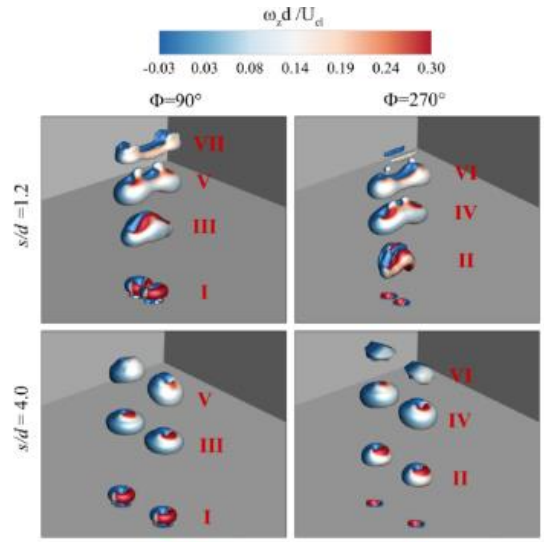

Figure 5. Phase-averaged vortical structures using iso-surfaces of the normalized Q-criterion ($Q^* = Qd/U_{cl} = 0.001$) colored with the normalized phase-averaged spanwise vorticity.

and 4 into two thin strips. In contrast, the rings in $s/d = 3.0$ and 4.0 are still independent during state II. As the evolution progresses through stages III-VII, the reoriented rings in $s/d = 1.2$ combine to form a single, elongated ring stretched in the crosswise (z) direction. Meanwhile, in $s/d = 4.0$, the initially separated rings gradually attract each other as they develop downstream.

B. Time-Averaged Flow Field.

Fig. 6 shows the contours of streamwise mean velocity (U_y/U_{cl}) and spanwise mean vorticity ($\omega_z d/U_{cl}$) for $s/d = 1.2$ and 4.0. In both cases, the velocity and vorticity are more intense in the near field and gradually decay further downstream due to the entrainment of surrounding fluid. The rate of decay tends to decrease as the spacing ratio increases. In $s/d = 1.2$ and 2.0, , the smaller spacing ratio promotes strong interactions between the inner shear layers of the TSJ leading to earlier merging and the formation of a single jet. In contrast, for $s/d = 3.0$ and 4.0, the TSJs converge toward each other; however, the merging of the inner shear layers and the formation of a single jet occurs further downstream.

The time-averaged turbulent kinetic energy, TKE is computed using the relation $TKE = 0.5(\widetilde{u_i'}\widetilde{u_i'}) + 0.5(\overline{u_i'u_i'})$ where $\widetilde{u_i'}$ is the periodic velocity fluctuations and u_i' is the random velocity fluctuations. Similarly, the in-plane Reynolds shear stress is determined $-uv = -\left(\widetilde{u_1'}\widetilde{u_2'} + \overline{u_1'u_2'}\right)$. Contours of normalized TKE and Reynold's shear stress for $s/d = 1.2$ and 4.0. are shown in Figure 7. For all cases, TKE is enhanced within the shear layers away from the jet-exits ($y/d \geq 4$). In $s/d = 1.2$, TKE is concentrated in a single core region but forms two lobes in $s/d = 3.0$ and 4.0 , due to reduced interaction between the jet as spacing ratio increases. Farther downstream, the TKE decays due to entrainment of the ambient fluid, however, the decay rate increases with decreasing spacing ratio.

The contours of the Reynolds shear stress reveal the shear layers within the TSJ. For $s/d = 1.2$, the TSJ exhibits an intense shear stress at the nozzle and peaks at $y/d = 2$, attributed to the effects of earlier merging of the inner shear layers of the jets. Moreover, the switch in signs of the Reynolds shear stress beyond $y/d = 5$ demonstrate the axis-switching behaviour. In contrast, for $s/d \geq 3.0$, the TSJ exhibits two separate pairs of Reynolds shear stress regions near the exit, which transitions to a single pair farther downstream due to the merging of the inner shear layers of the TSJ.

The decay of the TSJ is characterized using profiles of the local maximum streamwise mean velocity (U_m) of each jet. The profiles were similar for the TSJ due to symmetry; therefore, a single representative profile is presented for each test case in Fig. 8. The profiles of U_m/U_{cl} rapidly increases from the jet exit to a local maximum value and decay further downstream with increasing streamwise distance. The streamwise distance from the exit to the peak U_m/U_{cl} is often referred to as the potential core length (L_p). The value of $L_p/d = 1.5$ for $s/d = 1.2$ and 2.0 but increases to $L_p/d = 3.5$ for $s/d = 3.0$ and 4.0. The reduced potential core length for $s/d = 1.2$ and 2.0 is attributed to stronger inner shear layer interference between the TSJ. Except for $s/d = 2.0$, the decay rate tends to increase with decreasing spacing ratio.

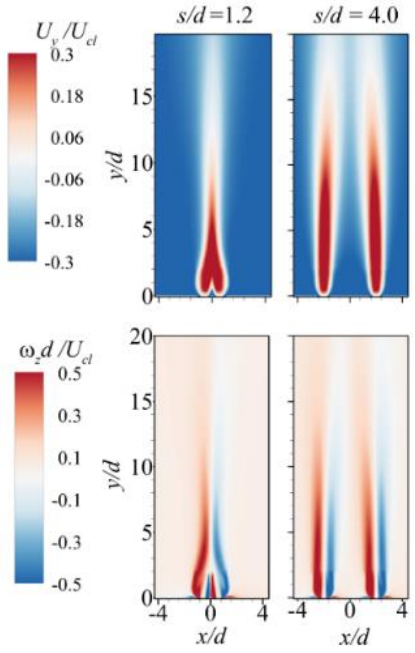

Figure 6. Contours of streamwise mean velocities and spanwise mean vorticity for s/d = 1.2 and s/d = 4.0.

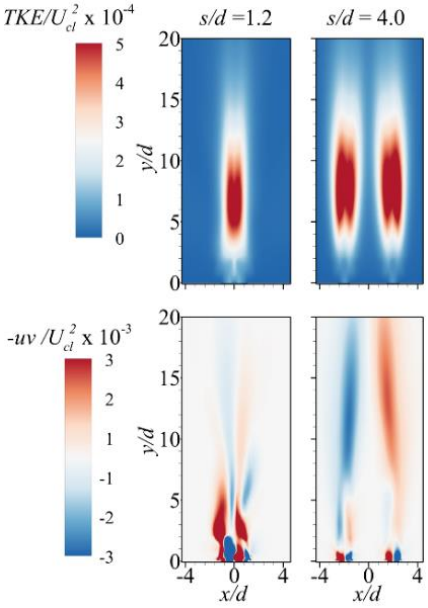

Figure 7. Contours of streamwise mean turbulent kinetic energy and Reynold's shear stresses mean vorticity for s/d = 1.2 and s/d = 4.0.

Profiles of U_m/U_{cl} and the local mean velocity along the symmetry line of the TSJ (i.e., at $x = z = 0$), U_{sym}/U_{cl} for $s/d = 1.2$ and 4.0 are shown in Fig. 9. These profiles are used to characterize the three main regions of the TSJ. The profiles of U_{sym}/U_{cl} exhibit negative velocities near the jet exit, which transitions to positive values and increases to values similar to U_m/U_{cl} downstream. The negative U_c/U_{cl} denote the converging region, which spans from the exit to the y_{mp}, determined as the location of $U_{sym}/U_{cl} = 0$. The streamwise location where $U_{sym} = U_m$ is determined as the combined point, y_{cp}. The profiles demonstrate that the converging and merging regions increase with increasing spacing ratio.

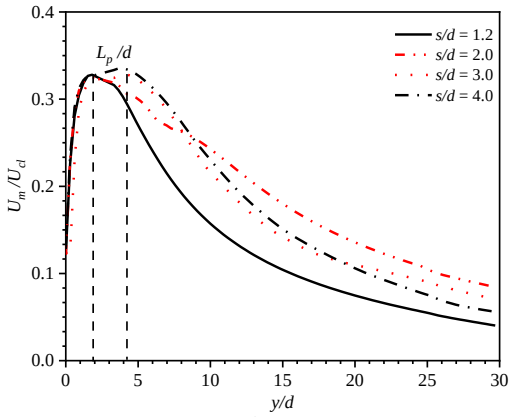

Figure 8. Streamwise evolution of the local maximum streamwise mean velocity for each jet for s/d = 1.2, 2.0, 3.0, 4.0.

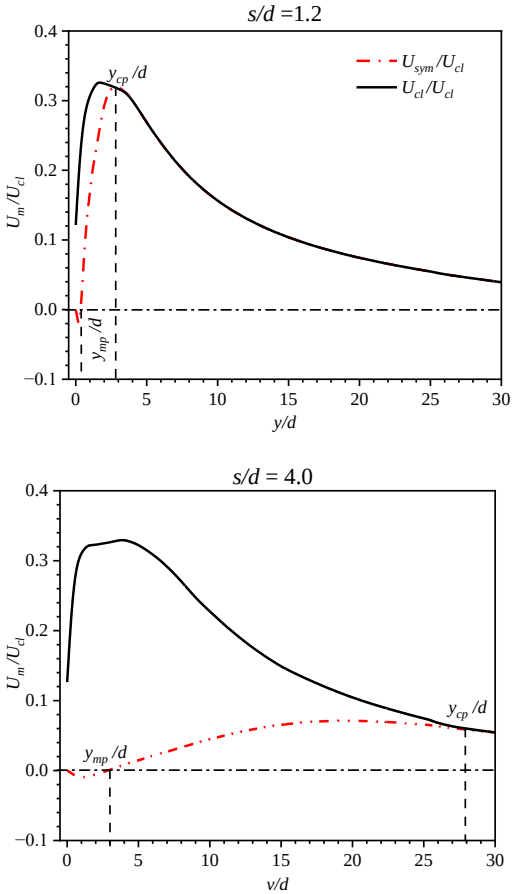

Figure 9. Streamwise evolution of the local maximum streamwise mean velocity and centerline velocity along the symmetry line for s/d = 1.2 and 4.0.

Fig. 10 shows that the distributions of y_{mp}/d and y_{cp}/d increases linearly with increasing spacing ratio, in agreement

with previous twin jet studies [2]. A least-squares line fitted to each dataset indicates the following correlation:

$$y_{mp}/d = 0.872(s/d) - 0.482 \quad (6)$$

$$y_{cp}/d = 9.614(s/d) - 10.047 \quad (7)$$

The trajectory of TSJ is examined using the loci of the local maximum velocity (U_m), as shown in Fig. 11. The streamwise distance is normalized by y_{cp}, while the spanwise distance is normalized by the spacing distance to scale the profiles of the four test cases. The plots demonstrate that each jet bends towards the symmetry line as it evolves downstream. A polynomial line fitted to the profiles of the four test cases shows that the trajectory can be described by:

$$x^* = 0.45724 + 0.04656(y^*) - 0.4579(y^*)^2 \quad (8)$$

where $x^* = x/s$ and $y^* = y/y_{cp}$.

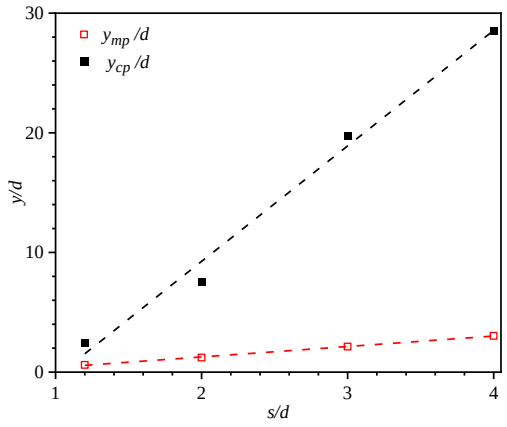

Figure 10. Distributions of y_{cp}/d and y_{mp}/d with increasing spacing ratio.

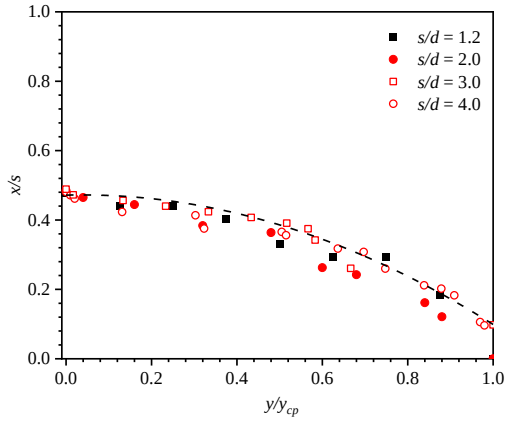

Figure 11. Loci of maximum streamwise mean for s/d = 1.2, 2.0 ,3.0,4.0

IV. Conclusion

The effect of spacing ratio on the interference of twin synthetic jets (TSJ) is investigated using IDDES. Four spacing ratios, s/d = 1.2, 2.0, 3.0 and 4.0, are examined at Reynolds number based on the maximum centerline jet-exit velocity of Re = 310. Contours of the time-averaged streamwise mean velocity showed that the TSJ exhibit three flow regions, similar to twin steady jets: converging, merging and combined regions, which are strongly influenced by the spacing ratio. The merging and combined points increased with increasing spacing ratio, while the decay rate of each jet decreased as the spacing ratio increased. The time-averaged turbulent kinetic energy and Reynolds shear stress demonstrated earlier turbulent mixing and faster decay of turbulence as spacing ratio decreased. The phase-averaged evolution of the 3D vortical structures revealed twin vortex rings that merge near exit for s/d = 1.2 and 2.0, subsequently undergoing axis-switching in the merging region of the TSJ. The re-oriented vortical structure is stretched in the combined region. In contrast, the vortex rings for s/d = 3.0 and 4.0 evolved independently, converging towards each other further downstream.

Acknowledgment

The authors are grateful to the Natural Sciences and Engineering Research Council of Canada (NSERC) for their financial support through a Discovery Grant for J.J. and E.E.E. We acknowledge the computational resources provided by the Digital Research Alliance of Canada and the Speed facilities at Concordia University.

References

[1] M. Kim, H. Lee, and W. Hwang, "Experimental study on the flow interaction between two synthetic jets emanating from a dual round orifice," *Exp. Therm. Fluid Sci*., vol. 126, pp. 110400, 2021.

[2] M. A. Feero, P. Lavoie, and P. E. Sullivan, "Influence of cavity shape on synthetic jet performance," *Sens. Actuators A Phys*., vol. 223, pp. 1–10, 2015.

[3] M. Ja'fari, F. J. Shojae, and A. J. Jaworski, "Synthetic jet actuators: Overview and applications," *Int. J. Thermofluids*, vol. 20, pp. 100438, 2023.

[4] A. Laban, S. S. Aleyasin, M. F. Tachie, and M. Koupriyanov, "Spacing effects on characteristics of round twin free jets," *Journal of Fluids Engineering*, vol. 141, Issue 7, pp. 071201, 2019.

[5] B. L. Smith and A. Glezer, "Vectoring of adjacent synthetic jets," *AIAA J*., vol. 43, No. 10, pp. 2117-2124, 2005.

[6] H. Li, N. Anand, Y. A. Hassan, and T. Nguyen, "Large eddy simulations of the turbulent flows of twin parallel jets," *Int. J. Heat Mass Transf*., vol.129, pp. 1263–1273, 2019.

[7] H. H. Ho, E. E. Essel, and P. E. Sullivan, "The interactions of a circular synthetic jet with a turbulent crossflow," *Phys. Fluids*, vol. 33, pp. 075108, 2022.

[8] X. K. Wang and S. K. Tan, "Experimental investigation of the interaction between a plane," Exp. Fluids, vol. 42, pp. 551-562, 2007.